Molecular Therapy
Nucleic Acids
Original Article

MicroRNA-145 Regulates Pathological Retinal Angiogenesis by Suppression of TMOD3

Chi-Hsiu Liu,[1] Zhongxiao Wang,[1] Shuo Huang,[1] Ye Sun,[1] and Jing Chen[1]

[1]Department of Ophthalmology, Boston Children's Hospital, Harvard Medical School, Boston, Massachusetts 02115, USA

Pathological angiogenesis is a hallmark of various vascular diseases, including vascular eye disorders. Dysregulation of microRNAs (miRNAs), a group of small regulatory RNAs, has been implicated in the regulation of ocular neovascularization. This study investigated the specific role of *microRNA-145* (*miR-145*) in regulating vascular endothelial cell (EC) function and pathological ocular angiogenesis in a mouse model of oxygen-induced retinopathy (OIR). Expression of *miR-145* was significantly upregulated in OIR mouse retinas compared with room air controls. Treatment with synthetic *miR-145* inhibitors drastically decreased levels of pathological neovascularization in OIR, without substantially affecting normal developmental angiogenesis. In cultured human retinal ECs, treatment with *miR-145* mimics significantly increased the EC angiogenic function, including proliferation, migration, and tubular formation, whereas *miR-145* inhibitors attenuated *in vitro* angiogenesis. Tropomodulin3 (TMOD3), an actin-capping protein, is a direct *miR-145* target and is downregulated in OIR retinas. Treatment with *miR-145* mimic led to TMOD3 inhibition, altered actin cytoskeletal architecture, and elongation of ECs. Moreover, inhibition of TMOD3 promoted EC angiogenic function and pathological neovascularization in OIR and abolished the vascular effects of *miR-145* inhibitors *in vitro* and *in vivo*. Overall, our findings indicate that *miR-145* is a novel regulator of TMOD3-dependent cytoskeletal architecture and pathological angiogenesis and a potential target for development of treatments for neovascular eye disorders.

INTRODUCTION

Angiogenesis, the formation of new blood vessels from existing ones, plays important roles in both physiological development and pathological conditions. The process of *de novo* vascular growth or neovascularization encompasses a series of morphogenic events, including sprouting, branching, lumen formation, anastomoses, and remodeling into a perfused vascular network, all of which require coordinated interaction of endothelial cells (ECs).[1] Dysregulated angiogenesis is associated with many diseases, including cardiovascular diseases, tumorigenesis, proliferative retinopathies, and neurodegeneration.[2] In retinopathy, pathological ocular neovascularization is characterized by a leaky, fragile, tuft-like appearance, which may cause retinal hemorrhage, leading to tractional retinal detachment and vision loss.[3] ECs play critical roles during angiogenesis, with those cells in the vascular growth front exposed to numerous angiogenic stimulators and inhibitors and following balanced guidance from these factors.[1,4] One of the most important factors in pathological angiogenesis—vascular endothelial growth factor (VEGF)—has been established as a key drug target in current anti-angiogenic therapies for cancers and neovascular eye diseases.[5] Yet anti-VEGF therapies are effective for some but not all patients and may affect normal vessel homeostasis.[6–8] Therefore, in designing improved targeted therapies for neovascular eye diseases, it is critical to identify additional factors controlling pathological angiogenesis, particularly those factors essential for the maintenance of normal vessel quiescence and transformation to proliferative neovessels under pathological conditions.

MicroRNAs (miRNAs) are a group of small (~22 nucleotides in length), endogenous, non-coding, regulatory RNA molecules.[9] miRNAs are involved in many biological processes, such as cell proliferation, cell death, neuronal differentiation and development, and angiogenesis.[10–16] miRNAs function through base pairing to the complementary sequence in the 3′ UTR of target mRNAs, to induce their cleavage and translational repression,[9] and hence are recognized as key mediators of post-transcriptional regulation through fine tuning gene expression. Previous studies have demonstrated the emerging role of miRNAs in vascular growth and neovascular diseases, including cancer and ocular angiogenesis.[16–26] In addition, work from several laboratories, including ours, has identified altered expression of multiple miRNAs in murine models of oxygen-induced retinopathy (OIR),[10,20,27] an experimental model characterized by ischemia-induced neovascularization in the retina. Specifically, expression of *miR-145*, a potential tumor suppressor,[28] is significantly upregulated in retinas in the OIR model.[27] *miR-145* is co-transcribed with *miR-143* as a cluster. Systematic *miR-145* knockout (KO) and *miR-143/145* double-KO mice are viable and show no overt abnormalities in cardiac structure and vascular smooth muscle cell differentiation.[29] Moreover, tumor-specific deletion of *miR-143/145* in a mouse model of lung adenocarcinoma exhibits diminished neovascularization and increased apoptosis, whereas wild-type mice injected with *miR-143/145*-expressing lung tumor cell lines develop aggressive lung tumors that are caused by stimulated proliferation of ECs.[30] In

Received 9 November 2018; accepted 13 March 2019;
https://doi.org/10.1016/j.omtn.2019.03.001.

Correspondence: Jing Chen, Department of Ophthalmology, Boston Children's Hospital, Harvard Medical School, Boston, Massachusetts 02115, USA.
E-mail: jing.chen@childrens.harvard.edu

the eye, *miR-143/145* cluster regulates corneal epithelium formation[31] and also intraocular pressure by modulating actin dynamics and contractility of trabecular meshwork.[32] However, the role of *miR-145* in pathological ocular angiogenesis and vascular endothelial function remains unclear.

In this study we investigated the potential role of *miR-145* as a novel post-transcriptional regulator controlling ocular neovascularization. Using a mouse model of OIR, we demonstrated that inhibition of *miR-145* reduces pathological angiogenesis in mouse retinas *in vivo*. *In vitro* administration of *miR-145* mimics increases vascular EC functions including proliferation, migration, and tubular formation, whereas *miR-145* inhibitors attenuate EC angiogenic functions. In addition, we identified tropomodulin 3 (*Tmod3*) as a novel target gene of *miR-145* and determined the targeting site of *miR-145* on the 3′ UTR of *Tmod3* by a luciferase reporter assay. We present evidence that *miR-145* represses *Tmod3* and that the *miR-145*/TMOD3 axis regulates EC morphology and cytoskeletal architecture *in vitro* and pathological vascular growth *in vivo*. Together, our findings indicate that inhibition of *miR-145* may serve as a potential therapeutic approach in developing treatments for pathological retinal angiogenesis.

RESULTS

miR-145 Is Highly Expressed in Mouse Retinas with OIR

Our previous analysis of miRNA expression array profiles showed an increase in *miR-145* levels by ~60% in pathological retinas with OIR,[27] a mouse model of proliferative retinopathy, by exposing neonatal mouse pups to 75% oxygen for 5 days from postnatal day 7 (P7) to P12, to induce maximal neovascularization at P17 (Figure 1A). We isolated total RNAs from mouse retinas with OIR and age-matched room air controls at various days (P7, P8, P12, P15, and P17) and evaluated *miR-145* expression levels by qPCR. Expression of *miR-145* revealed an increase during physiological development (Figure 1B, white bars). More importantly, in OIR retinas, *miR-145* expression levels decreased at P12, but significantly increased at P15 and P17 (Figure 1B, gray bars), compared with the levels in age-matched normoxic retinas, with no significant change at P8. Together, these data are consistent with our previous array results in which *miR-145* was upregulated in P17 retinas with pathological neovessels[27] and further validate dysregulation of *miR-145* in OIR, which may affect pathological vascular growth in retinopathy.

Inhibition of *miR-145* Suppresses Pathological Neovascular Growth

To determine whether *miR-145* influences pathological neovascularization in the OIR retinas, we performed intravitreal injection of *miR-145* inhibitors into OIR eyes at P12 after mice were removed from the oxygen. Vaso-obliteration (Figures 1C, 1F, and 1I) and neovascularization (Figures 1D, 1G, and 1J) were analyzed at P17. *miR-145* inhibitor treatment in OIR retinas significantly decreased the pathological neovascular area (by ~50%), compared with the contralateral eyes treated with negative controls (Figure 1D), without affecting vessel loss (Figure 1C). These results indicate that dysregulated *miR-145* affects the formation of pathological neovascularization in the mouse OIR model, and inhibition of *miR-145* alleviates the formation of neovessels.

Given the increase in *miR-145* expression during retinal development, we next examined the potential role of *miR-145* in developing retinal vessels. *miR-145* mimics or inhibitors were injected intravitreally into mouse eyes at P1, when mouse retinas are mostly devoid of blood vessels,[33] and retinal flat mounts were collected at P5. Quantification of superficial vascular coverage and density showed no significant difference in the retinas treated with exogeneous *miR-145* mimics compared with the contralateral eyes treated with negative controls (Figures 2A, top, 2B, and 2C). On the other hand, inhibition of *miR-145* revealed a modest decrease (~10%) in vascular density, with no significant difference in superficial layer vascular coverage (Figures 2E, top, 2F, and 2G). In addition, synthetic *miR-145* inhibitors were also injected intravitreally into P5 mouse retinas, when the superficial retinal vessels had partially developed, and the retinal vascular areas were analyzed at P7. No significant vascular changes were observed with *miR-145* inhibitor treatment at P7 (Figures 2E, center, 2H, and 2I). Moreover, to evaluate the effects of *miR-145* during the development of the deep retinal vascular plexus, *miR-145* mimics or inhibitors were injected intravitreally into P6 mouse eyes, and the deep-layer vasculature was observed at P10. Neither supplement of exogenous *miR-145* mimics (Figures 2A, bottom, and 2D) nor inhibition of *miR-145* (Figures 2E, bottom, and 2J) affected the development of deep retinal vessels significantly. These results suggest that, although *miR-145* is critical for pathological neovascularization, it has little or minimal influence on normal retinal capillary development and vascular expansion.

Modulation of *miR-145* Alters Vascular EC Angiogenic Functions

To further address the role of *miR-145* in angiogenesis, we used *ex vivo* aortic ring culture treated with *miR-145* mimics to investigate its effects on EC sprouting (Figures 3A and 3B). Aortic explants treated with *miR-145* mimics revealed a significant increase in endothelial sprouting areas compared with the negative control oligomer-treated group (Figure 3B), suggesting that *miR-145* promotes angiogenesis *ex vivo*.

We next examined whether *miR-145* directly regulates EC angiogenic functions in human retinal microvascular endothelial cells (HRMECs). Treatment with *miR-145* mimics substantially promoted HRMEC proliferation, tube formation, and migration (Figures 3C–3F). An approximately 14% increase in proliferation (Figure 3D), an 80% increase in tubular formation in mesh areas (Figure 3E), and a >2.7-fold increase in migration distance (Figure 3F) were observed with *miR-145* mimic treatment. On the other hand, inhibition of *miR-145* significantly decreased EC tube formation and migration (Figures 3C, 3E, and 3F), indicating direct pro-angiogenic effects of *miR-145* on EC functions.

Tmod3 Is a Direct Target Gene of *miR-145*

miRNA functions by regulating target gene expression post-transcriptionally by binding to the conserved seed sequences in the 3′

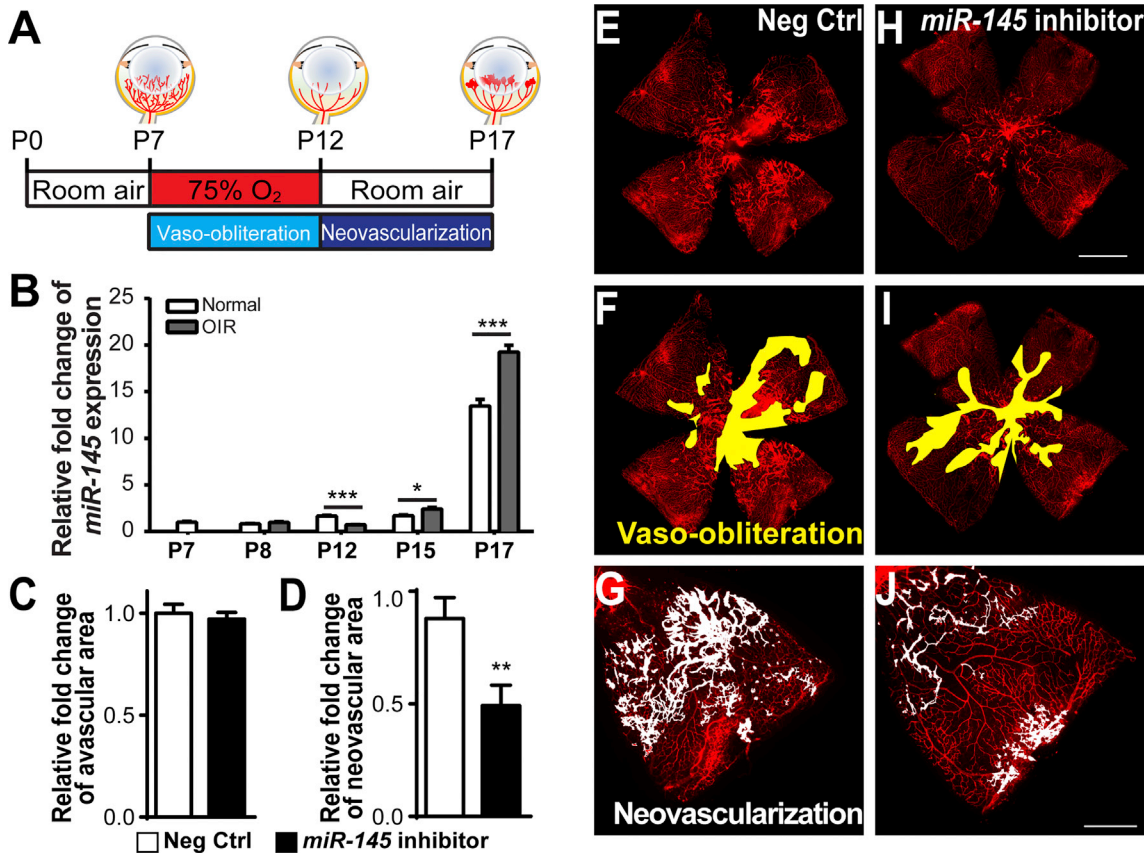

Figure 1. *miR-145* Suppresses Pathological Neovascularization in Mouse Retinas with Oxygen-Induced Retinopathy

(A) Schematic diagram of the oxygen-induced retinopathy (OIR) model. Neonatal mice were exposed to 75% of oxygen from postnatal day 7 (P7) to 12. Vessel loss was induced during oxygen exposure, and maximal neovascularization was induced at P17, 5 days after the mice were returned to room air. (B) Expression levels of *miR-145* were analyzed in OIR retinas compared with age-matched room air control retinas at different time points. *MiR-145* expression was significantly reduced in OIR retinas at P12, yet was upregulated at both P15 and P17 compared with normoxic retinas, normalized to *U6* small nuclear RNA (snRNA) as the control (n = 6 per group). (C–J) Intravitreal injection of the *miR-145* inhibitor or the non-targeting negative control was performed in OIR mouse eyes at P12, with the *miR-145* inhibitor injected into one eye and the negative control in the contralateral eye, followed by analysis of the retinal vasculature at P17. Quantitative analysis of vaso-obliteration (C) and pathological neovascularization (D) showed that *miR-145* inhibitor treatment significantly reduced neovascularization in OIR retinas compared with negative control treatment of contralateral retinas, with no significant difference in vaso-obliteration (n = 16 per group). Representative retinal whole mounts were stained with *Griffonia simplicifolia* isolectin B_4 (IB_4) from P17 OIR mice with injection of negative control (E) or *miR-145* inhibitor (H); areas of vaso-obliteration (F, negative controls, and I, *miR-145* inhibitor) and neovascular tufts (G, negative controls, and J, *miR-145* inhibitor) are labeled in yellow and white, respectively. Scale bars represent 1 mm (B) and 500 μm (F). Neg Ctrl, negative control RNA oligomers. Data are presented as means ± SEM. *$p \leq 0.05$; **$p < 0.005$; ***$p \leq 0.001$.

UTR of mRNA.[34] We performed *in silico* analysis of putative *miR-145* target genes based on the conservation of seed sequence matches across human and mouse, which identified Krüppel-like factor 4 (*Klf4*), semaphorin 3A (*Sema3a*), TMEM9 domain family member B (*Tmem9b*), *Tmod3*, and trio Rho guanine nucleotide exchange factor (*Trio*) as potential *miR-145* targets with base pairing to the conserved seed sequences (UCCAGUUU). Consistent with *miR-145* upregulation at P17 in OIR (Figure 1B), *Klf4*, *Tmem9b*, *Tmod3*, and *Trio* are all significantly decreased in the P17 OIR retinas, as was the known *miR-145* target gene *c-Myc* (Figure 4A).

To confirm whether these candidate genes are directly targeted by *miR-145*, we performed a luciferase reporter assay in HEK293T cells by cloning the 3′ UTR containing *miR-145* seed sequences of *Klf4*, *Sema3a*, *Tmem9b*, *Tmod3*, and *Trio* into the pmirGLO vector (Figure 4B). The most significant reduction of luciferase activity by *miR-145* mimic treatment was observed in cells transfected with *Tmod3* constructs, revealing a >4-fold reduction in a dose-dependent manner (Figure 4C), with *Tmem9b* constructs also showing reduction to a lesser extent and no significant changes in the other gene constructs (Figure 4C). TMOD3 regulates EC migration by capping the pointed ends of actin filaments and blocking their elongation and depolymerization, thereby influencing actin cytoskeletal structure and dynamics in lamellipodia.[35,36] TMEM9B is a positive regulator of inflammatory cytokines.[37] Our findings of *miR-145* modulation of EC proliferation, migration, and tubular formation (Figure 3) are

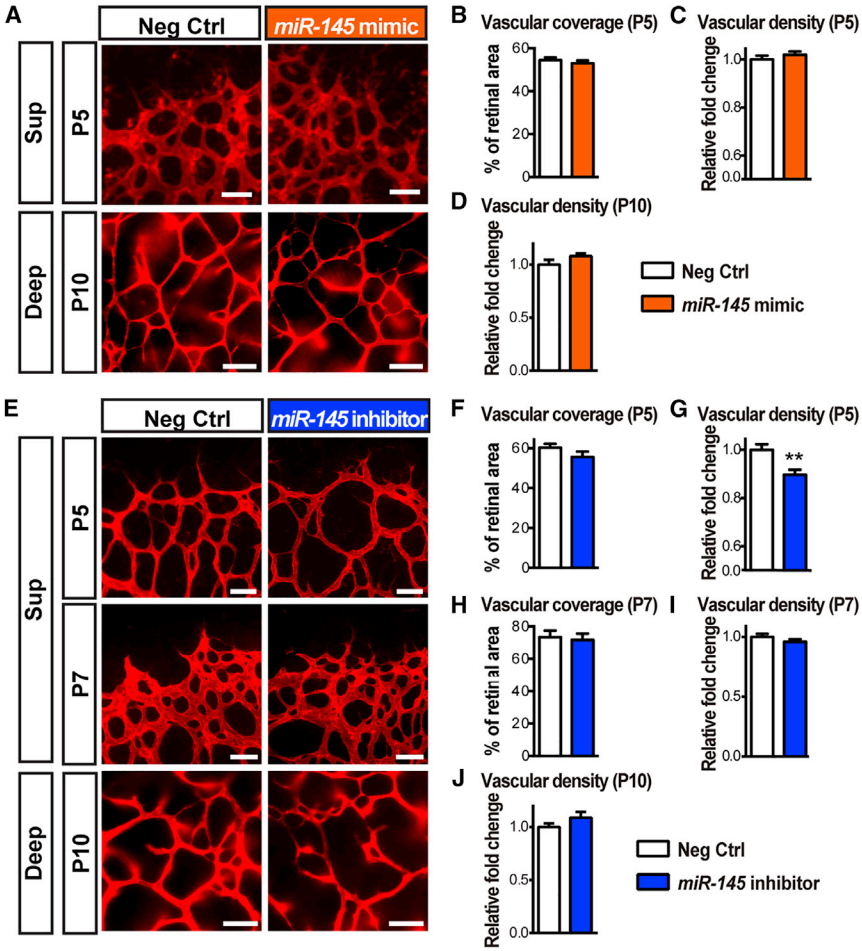

Figure 2. Minimal Effects of *miR-145* on Developmental Retinal Angiogenesis

(A) Representative images of P5 and P10 mouse retinas treated with *miR-145* mimics or negative control oligomers via intravitreal injection at P1 and P6, respectively, followed by staining with IB_4 for observing the superficial (at P5, top) and deep (at P10, bottom) vascular layers. (B–D) Quantification of vascularized retinal areas (B, at P5) and vascular density (C, at P5, and D, at P10) in the negative control- and *miR-145* mimic-treated groups show no significant difference. (E) Representative images of IB_4-stained P5, P7, and P10 retinas treated with *miR-145* inhibitors or negative controls at P1, P5, and P6, respectively. (F–J) Analyses of the vascularized areas of superficial retinas (F and H) and the vascular density of the superficial vasculature (G and I) or the deep vascular plexus (J) revealed no significant difference in the superficial retinal areas (P5, F, and P7, H) and vascular density (P7, I; P10, J) between the control- and *miR-145* mimic-treated retinas (P5 and P7: n = 13 or 16 mice per group; P10: n = 7 or 8 mice per group), with very modest reduction of vascular density at P5 (G). Scale bars represent 50 μm (A and E), P5 and P7, and 100 μm (A and E), P10. Deep, deep retinal vascular layer; Neg Ctrl, negative control RNA oligomers; Sup, superficial retinal vascular layer. Data are presented as means ± SEM. $^{**}p \leq 0.005$.

highly related to the known angiogenic functions of TMOD3 in ECs; hence, we focused on TMOD3.

We next investigated whether TMOD3 protein levels are altered in OIR and, by *miR-145* modulation, in HRMECs. In P17 OIR retinas, TMOD3 protein levels were decreased by ~70% compared with normoxic retinas (Figures 4D and 4E), confirming downregulated *Tmod3* mRNA levels in OIR (Figure 4A) and consistent with OIR induction of *miR-145* (Figure 1B). Moreover, hypoxia treatment of HRMECs significantly induced *miR-145* expression and also decreased TMOD3 protein levels (Figures 4F and 4G), suggesting that their regulation in OIR was likely hypoxia responsive. In addition, HRMECs treated with *miR-145* mimics showed drastically decreased TMOD3 expression (by up to 90%), whereas cells treated with *miR-145* inhibitors had substantially increased expression levels of *TMOD3* (by ~2-fold; Figure 5A). Importantly, TMOD3 protein levels demonstrated significant dose-dependent reduction after treatment with *miR-145* mimics (Figures 5B and 5C). Together, these data confirm that *Tmod3* is a primary target gene suppressed by *miR-145* in vascular ECs and may thereby mediate the vascular effects of *miR-145*.

miR-145 Affects EC Morphology and Cytoskeletal Architecture through TMOD3

We next asked whether downregulation of *Tmod3* by *miR-145* alters EC morphology and functions. Because the canonical function of TMOD3 is as a regulator that caps actin filaments and modifies the dynamics and architecture of the actin network,[35] we examined whether *miR-145* induces alteration of EC functions via TMOD3-dependent morphological changes in the EC cytoskeleton. HRMECs were treated with negative controls or *miR-145* mimics for 72 h, and the cells were live imaged prior to immunostaining with TMOD3 and F-actin. Significant morphological changes were observed in the *miR-145* mimic-treated cells, showing decreased levels of TMOD3 staining, marked elongation of cell shape, and less organized actin meshwork (Figure 5D). In addition, measurement of both the length and width of ECs revealed a substantial increase in cell length and significantly higher aspect ratios (length versus width) in the *miR-145* mimic-treated group compared with the negative controls (Figure 5E).

To evaluate the role of TMOD3 in mediating the effects of *miR-145* on EC functions, we performed co-transfection of small interfering RNA (siRNA) targeting *Tmod3* (siTMOD3) and *miR-145* inhibitors to HRMECs. Treatment with siTMOD3 significantly suppressed (by ~50%) *Tmod3* expression in HRMECs, compared with negative control siRNA (siNC) (Figure 6A), confirming successful knockdown. Treatment with siTMOD3 significantly promoted HRMEC proliferation and angiogenic function (Figures 6B and 6C) and caused

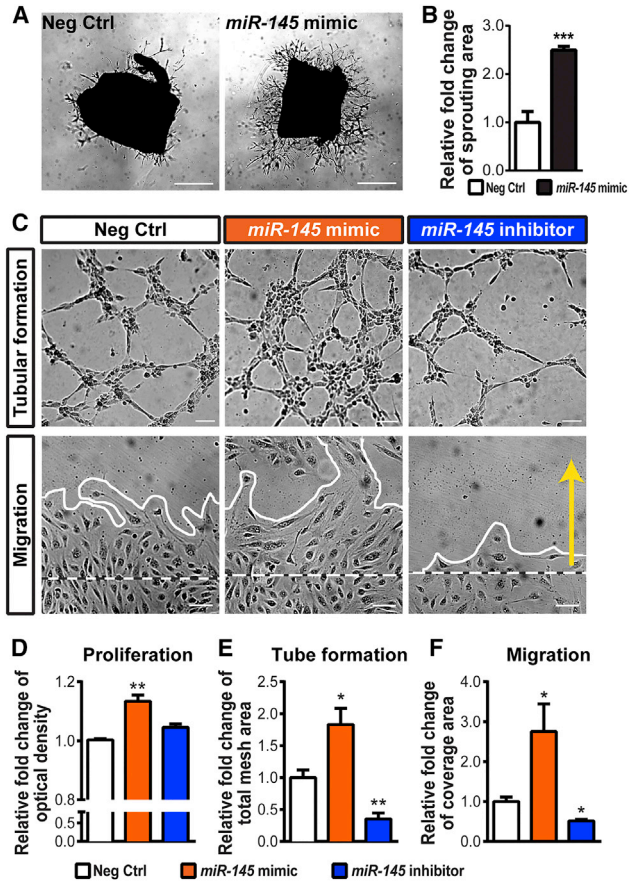

Figure 3. *miR-145* Increases Endothelial Angiogenic Functions

(A) Representative images of vascular sprouting from aortic rings isolated from P20 mice. Tissue explants were treated with a non-targeting negative control (left) or the *miR-145* mimic (right). (B) Quantitative analysis of the sprouting area in day 4 explants showed that the *miR-145* mimic significantly increased sprouting ability *ex vivo* compared with rings treated with the negative control (n = 6–9 per group). (C–F) Human retinal microvascular endothelial cells (HRMECs) were treated with the *miR-145* mimic, inhibitor, or negative control and analyzed for endothelial functions. Representative images (C) show tubular formation (top) and results of a wound-healing migration assay (bottom; white dashed lines indicate the initial boundaries of the scratches, white solid lines show the leading edges at 24 h after treatment, and the yellow arrow indicates the direction of cell migration). Quantitative analyses show that HRMECs treated with the *miR-145* mimic displayed higher levels of proliferative activity in an MTT assay (D), mesh areas in a tube-formation assay (E), and cell coverage areas during migration (F), compared with cells treated with the negative control. Inhibition of *miR-145* in HRMECs reveals significantly decreased levels of tube formation (E) and migration (F). (D) n = 3 per condition; (E and F) n = 6 per group. Scale bars represent 1 mm (A) and 100 μm (C). Neg Ctrl, negative control RNA oligomers. Data are presented as means ± SEM. *$p \leq 0.05$; **$p \leq 0.005$; ***$p < 0.001$.

morphological cytoskeleton changes, including distinctly elongated cell shapes with increased aspect ratio and less organized actin mesh (Figures 6D and 6E), similar to the vascular phenotypes observed in *miR-145* mimic-treated cells (Figures 3C–3F and 5). Moreover, co-treatment with siTMOD3 and *miR-145* inhibitors significantly reversed the effects of *miR-145* inhibitors on endothelial angiogenic function (Figure 6C). These data indicate that *miR-145* influences the vascular EC cytoskeletal meshwork and morphologic changes important for EC sprouting and angiogenesis and that the vascular effects of *miR-145* are mediated largely through TMOD3.

Inhibition of TMOD3 Exacerbates Neovessel Formation and Reverses the Vascular Effects of *miR-145* in OIR

To further verify the neovascular effect of *Tmod3 in vivo*, we intravitreally injected siTMOD3, alone or in combination with *miR-145* inhibitors, into OIR mouse eyes at P12 and analyzed the pathological vasculature at P17. siTMOD3 treatment suppressed the retinal expression of *Tmod3* by ~50% (Figure 7A) and led to a substantial increase of neovascularization in the OIR mouse eyes compared with contralateral siNC injection (Figures 7B–7D), supporting the anti-angiogenic effects of TMOD3 *in vivo*. Moreover, *miR-145* inhibitor treatment increased the retinal expression of *Tmod3* by ~3-fold *in vivo* (Figure 7E), and siTMOD3 co-treatment with *miR-145* inhibitors significantly induced neovascularization in OIR, hence reversing the anti-angiogenic effects of *miR-145* inhibitors in OIR (Figures 7F–7H) and suggesting that the vascular effects of *miR-145* on pathological neovascularization in OIR (Figure 1D) is mediated in part by its regulation of *Tmod3*. Overall, our results indicate that the *miR-145*/TMOD3 axis plays a significant role in regulating neovascularization in OIR.

DISCUSSION

In this report, we present findings that retinal *miR-145* is a key regulator of EC actin dynamics and cell structure during pathological ocular neovascularization through post-transcriptional control of *Tmod3*. In the ischemia-induced experimental retinopathy, upregulated *miR-145* repressed the expression of *Tmod3*, causing alleviation of TMOD3 binding to the pointed ends of actin filaments that allowed its elongation and depolymerization, thereby leading to alterations in EC cytoskeletal architecture and dynamics, which may affect pathological angiogenic sprouting (Figure 8).

Our previous study in the mouse model of OIR identified a significant increase of retinal *miR-145* during the neovascular phase,[27] indicating that dysregulation of *miR-145* may be linked to pathological retinal angiogenesis. Here, we found that *miR-145* increased gradually in the neonatal mouse retinas during physiological development and was robustly upregulated in the OIR retinas during formation of neovascular tufts in the second hypoxia phase (Figure 1). Upregulation of *miR-145* during the neovascular phase of OIR likely reflects its hypoxia-responsive nature, where in HRMECs *miR-145* was upregulated in the hypoxic condition (Figure 4F and 4G). This observation is consistent with previous studies in bladder cancer, indicating that *miR-145* is a hypoxia-regulated miRNA targeting by hypoxia-inducible factor-1 alpha subunit (HIF-1α),[38] which also regulates transcription of angiogenic genes in the mouse OIR model and human retinopathy.[39] On the other hand, the increasing expression of *miR-145* during retinal development may correlate with the retinal maturation process and may reflect in part potential physiological hypoxia during development, in addition to induction by other signaling pathways,

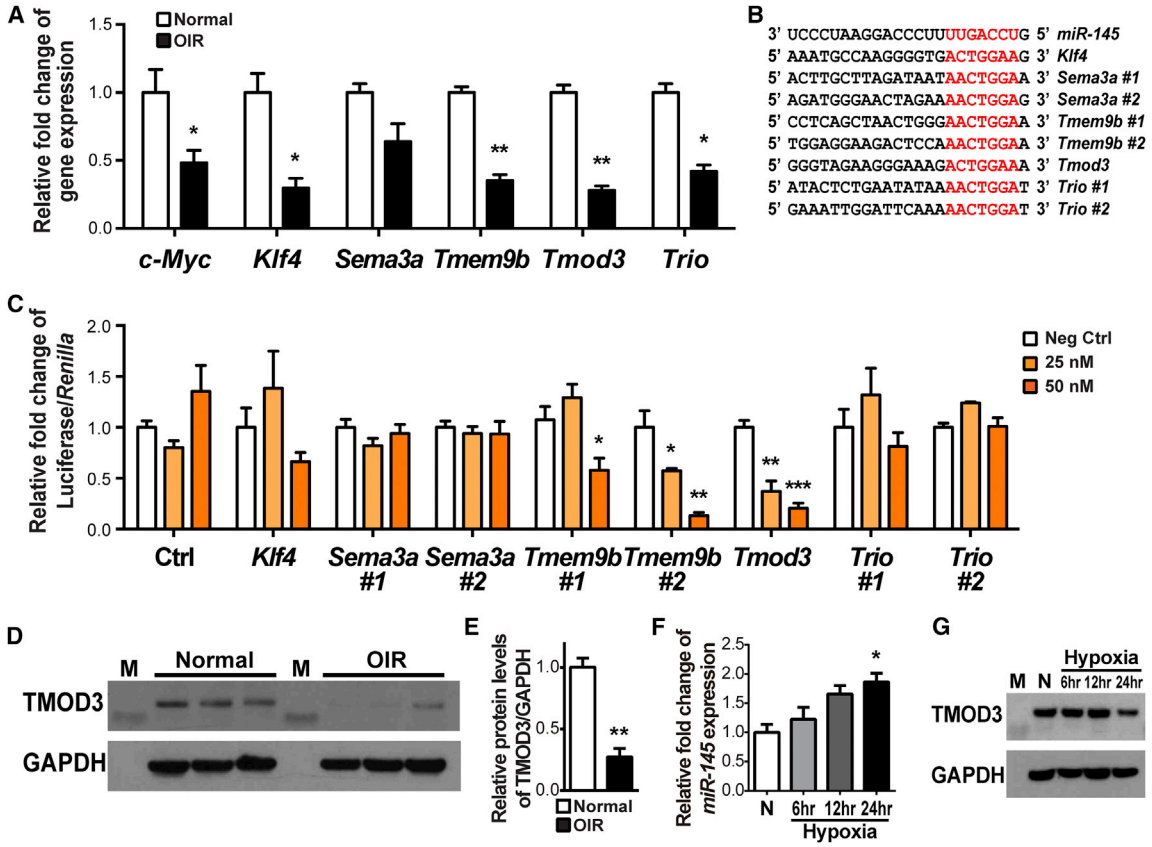

Figure 4. *Tmod3* Is a Target Gene of *miR-145*

Candidate target genes *of miR-145*—Krüppel-like factor 4(*Klf4*), semaphorin 3A (*Sema3a*), TMEM9 domain family member B (*Tmem9b*), tropomodulin 3 (*Tmod3*), and trio Rho guanine nucleotide exchange factor (*Trio*)—were identified by analyzing the seed sequence of *miR-145*, conserved in both human and murine, for sequence complementarity to determine predicted target mRNAs. (A) Expression levels of *Klf4*, *Tmem9b*, *Tmod3*, and *Trio* were significantly downregulated in P17 OIR retinas compared with normoxic control retinas (n = 6 per group). *c-Myc*, a known *miR-145* target gene, served as the positive control. Expression levels were normalized to *18S* and then to the levels in normoxic retinas. (B) The sequence alignment between mouse *miR-145* and the putative binding sites in the 3′ UTR of target genes, with sequences recognized by the *miR-145* seed sequence shown in red. (C) Luciferase reporter assays of putative *miR-145* target genes were performed in HEK293T cells. Cells were transfected with 25 or 50 nM of *miR-145* mimics or the negative control, and each was co-transfected with constructs of luciferase reporter containing *miR-145* target sequences of *Klf4*, *Sema3a*, *Tmem9b*, *Tmod3*, and *Trio*. Cells transfected with the *Tmod3* target sequence resulted in significant repression of luciferase activity in a *miR-145* dose-dependent pattern (n = 3–6 per group). Firefly luciferase activities were normalized to the *Renilla* luciferase and to the levels in the negative control. (D and E) Western blotting shows the expression of TMOD3 and glyceraldehyde 3-phosphate dehydrogenase (GAPDH) in P17 OIR and normoxic control retinas. (E) Densitometric quantification shows that TMOD3 protein levels were substantially decreased in P17 OIR retinas compared with normoxic controls. GAPDH served as the internal loading control (n = 3 per group). (F) *miR-145* expression levels were analyzed by real-time qPCR using total RNA obtained from HRMECs exposed to hypoxia for the indicated period of time. *miR-145* expression was elevated over time in hypoxic HRMECs. *miR-145* expressing levels were normalized to *U6* snRNA and normoxia controls (n = 3 per group). (G) TMOD3 protein levels in HRMECs exposed to hypoxia for the indicated period of time were detected by western blot assay. GAPDH expression was used as a loading control. M, molecular weight markers; N, normoxia. Data are presented as means ± SEM. *$p \leq 0.05$; **$p \leq 0.005$; ***$p \leq 0.001$.

such as serum response factor (SRF)[29] and Notch.[40] Previous studies demonstrated that activation of *miR-143/145* could be regulated in parallel by SRF-dependent networks and Notch1 intracellular domain-containing complexes.[29,40] Both signaling pathways have been shown to be important in retinal vascular development and association with the pathogenesis of neovascular eye diseases.[29,40–46]

miR-145 is often co-transcribed with *miR-143* and has been reported to be one of the most abundantly expressed miRNAs in vascular walls in arteries and in smooth muscle cells.[28,47] Expression of *miR-145* is significantly downregulated, both in atherosclerosis in humans and in a rat model of arterial balloon injury.[47,48] In addition to smooth muscle cells, *miR-143/145* is also expressed in vascular ECs and at low levels in normoxic cultured ECs,[28] consistent with our finding of low *miR-145* levels in normoxic retinas and suggesting that steady and low levels of *miR-145* is sufficient in maintaining EC quiescence. On the other hand, *miR-143/145*-deficient mice show attenuated tumor angiogenesis and limited tumor expansion, suggesting that loss of *miR-143/145* from the tumor microenvironment suppresses tumor neoangiogenesis.[30] In line with this pro-angiogenic role of

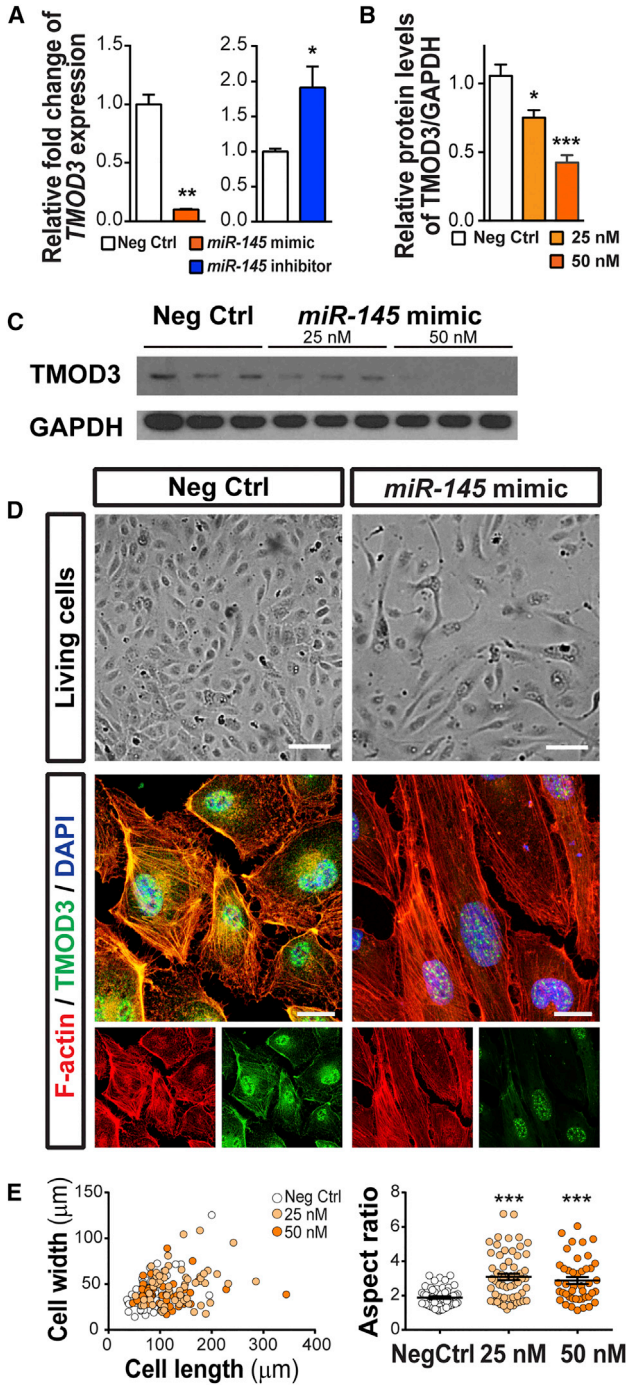

Figure 5. *miR-145* Suppresses TMOD3 Protein Levels and Affects EC Actin Cytoskeleton and Morphology

(A) Treatment of *miR-145* mimics significantly decreased expression of *TMOD3* in HRMECs, whereas *miR-145* inhibitors increased expression of *TMOD3*, confirming that the *Tmod3* gene is a direct target of *miR-145* in vascular ECs. Expression levels were normalized to *18S* and to cells treated with negative control (n = 3 per group). (B and C) Western blot analysis of TMOD3 and GAPDH in HRMECs transfected with *miR-145* mimics (25 or 50 nM) or negative controls for 72 h. (C) Densitometric analysis shows that TMOD3 protein levels were substantially decreased in HRMECs treated with *miR-145* mimics dose-dependently. GAPDH serves as internal loading control (n = 6–9 per group). (D) Representative images of living cells (top) and immunocytochemical staining (bottom) of F-actin (red) and TMOD3 (green) in HRMECs treated with *miR-145* mimics or negative controls. Live HREMCs treated with *miR-145* mimics showed morphological change with an elongated appearance; moreover, immunofluorescence imaging revealed decreased TMOD3 staining, longer F-actin fibers and less cytoskeleton mesh, and elongation of cell shape in the mimic-treated group. (E) Quantification of cell morphology by measuring individual cell width and length. Each dot represents one cell. The left graph shows that HRMECs treated with *miR-145* mimics had increased cell length. The right shows the aspect ratio (cell length/cell width) of HRMECs with the different treatments. Cells treated with *miR-145* mimics had a significantly increased aspect ratio compared with negative control-treated cells (n = 45–70 cells/group). Scale bars represent 100 μm (D, top) and 20 μm (D, bottom with immunocytochemical staining). Neg Ctrl, negative control RNA oligomers. Data are presented as means ± SEM. ***$p \leq 0.001$.

miR-143/145, we found that treatment with *miR-145* inhibitors intravitreally injected into OIR mouse eyes significantly suppressed neovascularization (Figure 1), indicating that *miR-145* induction in retinopathy may be a key pathogenic factor contributing to pathological retinal neovascularization. In addition, *miR-145* mimic treatment promoted angiogenesis both in murine aortic ring explants and in cultured human ECs (Figure 3), further supporting the pro-angiogenic function of *miR-145*.

Our study identified *Tmod3* as a novel direct target gene of *miR-145*, supported by the findings that modulation of *miR-145* significantly altered *Tmod3* levels *in vitro* and *in vivo* (Figures 4, 5, and 7). The TMOD family is a group of proteins that cap the slow-growing (pointed) ends of actin filaments, blocking their elongation and depolymerization, hence regulating the stability, length, and architecture of the actin cytoskeleton.[35] Four TMOD isoforms are expressed in vertebrates in a tissue-specific and developmentally regulated manner. Vascular ECs contain only TMOD3, associated with the dynamic actin filament network in ECs.[36] During angiogenesis, rapid remodeling of EC actin filament networks occurs, in response to signaling cascades elicited by growth stimuli or environmental cues.[49] Fischer et al.[36] reported that TMOD3 is a negative regulator of the EC motility in human microvascular ECs. Their study localized TMOD3 to the actin filament, found it to be specifically enriched in the leading lamellipodia of ECs, and showed that modulation of TMOD3 altered free pointed and barbed ends in the lamellipodial actin filaments, concomitant with altered EC motility.[36] Moreover, a previous study in adipocytes showed that TMOD3 is an AKT2 effector, mediating insulin-induced cortical actin remodeling.[50] In line with this evidence, we found that exogenous *miR-145*-treated human retinal ECs showed diminished *Tmod3* expression in the actin filaments and altered EC actin dynamics and cell structure (Figure 5), associated with increased ability for cell proliferation, tubular formation, and cell migration (Figure 3). TMOD3 inhibition mimicked the vascular effects of *miR-145* and reversed the effects of *miR-145* inhibitors *in vitro* and *in vivo*, suggesting that the vascular effects of *miR-145* on EC functions and in OIR are likely mediated via its transcriptional regulation of *Tmod3*.

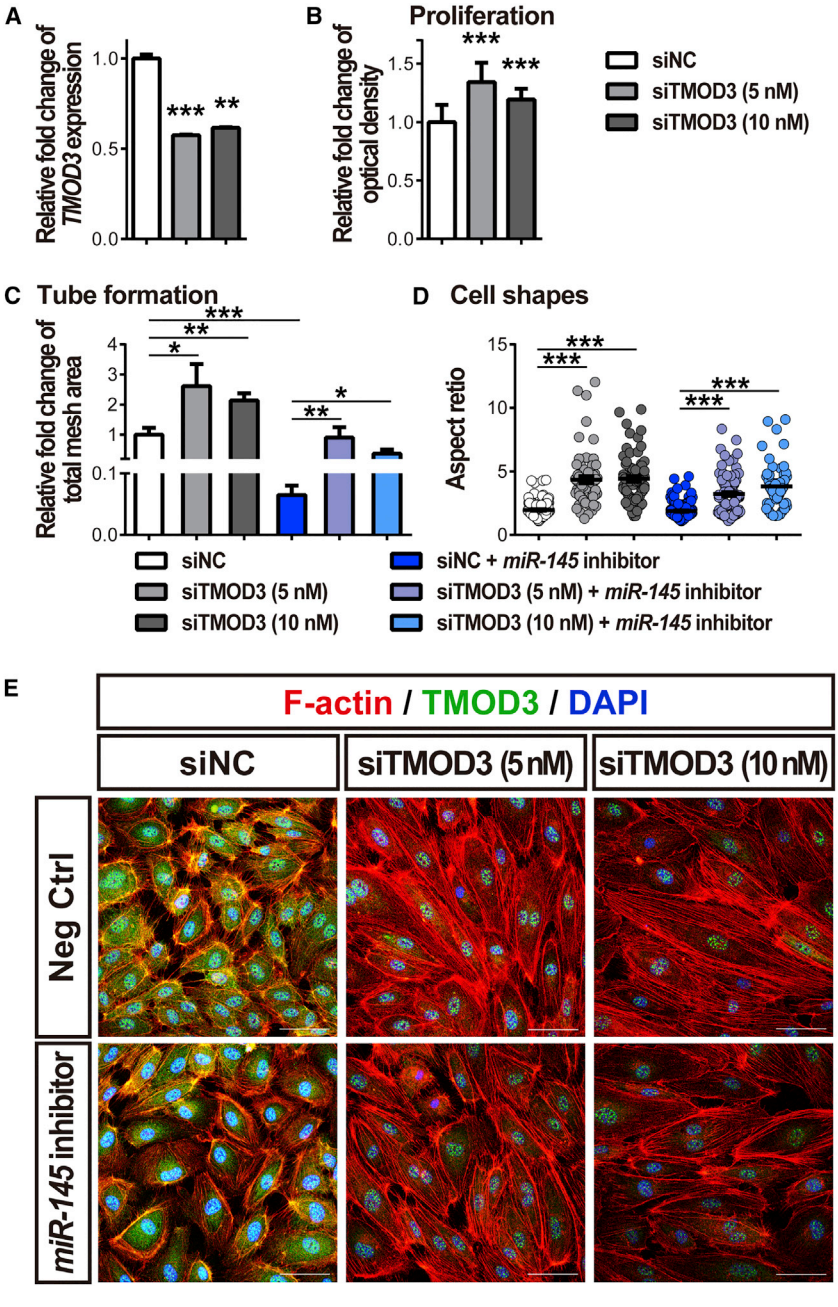

Figure 6. TMOD3 Mediates EC Functions and Cytoskeletal Morphology

(A and B) HRMECs were transfected with small interfering RNA (siRNA) targeting *TMOD3* (siTMOD3) (5 or 10 nM) or negative control siRNA (siNC) for 24 h. (A) Treatment of siTMOD3 significantly decreased expression of *TMOD3* in HRMECs. Expression levels were normalized to *18S* and to cells treated with siNC (n = 3 per group). (B) Quantitative analyses of MTT assays showed that HRMECs treated with siTMOD3 had significantly increased proliferative activity (n = 9–12 per condition). (C and E) HRMECs were transfected with *miR-145* inhibitors (50 nM) or negative controls (Neg Ctrl) combined with siTMOD3 (5 or 10 nM) or siNC for 24 or 48 h and analyzed for tube formation (C) and cell shape (D and E). In the tube formation assay, HREMCs transfected with siTMOD3 had a significant increase in total mesh area, even in the *miR-145* inhibitor co-transfected groups (C); n = 6 cells per group. Furthermore, knockdown of TMOD3 in HRMECs show a substantially increased aspect ratio (cell length/cell width) indicating elongated cell shape compared with cells treated with siNC (D); n = 60–130 cells per group. Immunocytochemical staining of F-actin (red) and TMOD3 (green) in HRMECs demonstrated decreased TMOD3 staining, longer F-actin fibers, less cytoskeleton mesh, and elongation of cell shape in the siTMOD3-treated group (E). Scale bars represent 50 μm (E). Data are presented as means ± SEM. *$p \leq 0.05$; **$p \leq 0.005$; ***$p < 0.001$.

Work in *miR-145* KO and *miR-143/145* double-KO mice showed notably thinner smooth muscle layers of the arteries, with a decreased number and prominence of stress fibers in the smooth muscle cells.[29] It is suggested that the absence of *miR-143/145* causes an imbalance of cytoskeletal homeostasis, thereby perturbing stress fiber formation and actin remodeling, resulting in altered cell morphology.[29] Previous studies found expression of *miR-143/145* in multiple cell types in the eyes, including vascular smooth muscle cells, pericytes, ciliary muscles, extraocular muscles, photoreceptors, and Müller glia.[32,51] *miR-143/145* regulates actin dynamics and the contractility of cells in the trabecular meshwork to affect eye pressure.[32] *miR-145* also plays an important role in the TGF-β1-stimulated corneal myofibroblast activity and contractility that affects corneal scaring.[52] In our study, we found that exogenous *miR-145* influenced cytoskeletal architecture and caused elongation of cell shapes in cultured human retinal ECs (Figure 5). These findings suggest that *miR-145* regulates its downstream targets, including *Tmod3*, in multiple cell types to induce actin cytoskeletal changes in diverse tissues.

Together, our data link *miR-145* and *Tmod3* with EC functional change, which may underlie the vascular effects of *miR-145* on pathological ocular angiogenesis in OIR. In OIR retinas, hypoxia-induced *miR-145* expression may enhance neovascular sprouting growth by repression of *Tmod3* and thereby influence EC actin remodeling in the angiogenic front to enhance neovascular sprouting (Figure 8). Yet potential contribution from other target genes such as *Tmem9b*, an inflammatory regulator,[37] cannot be excluded. Inflammatory changes also occur in retinopathy and contribute to neovascular response, and *miR-145* may also exert anti-inflammatory effects via *Tmem9b* to dampen inflammation and suppress in part the neovascular response in OIR, an effect that awaits further investigation.

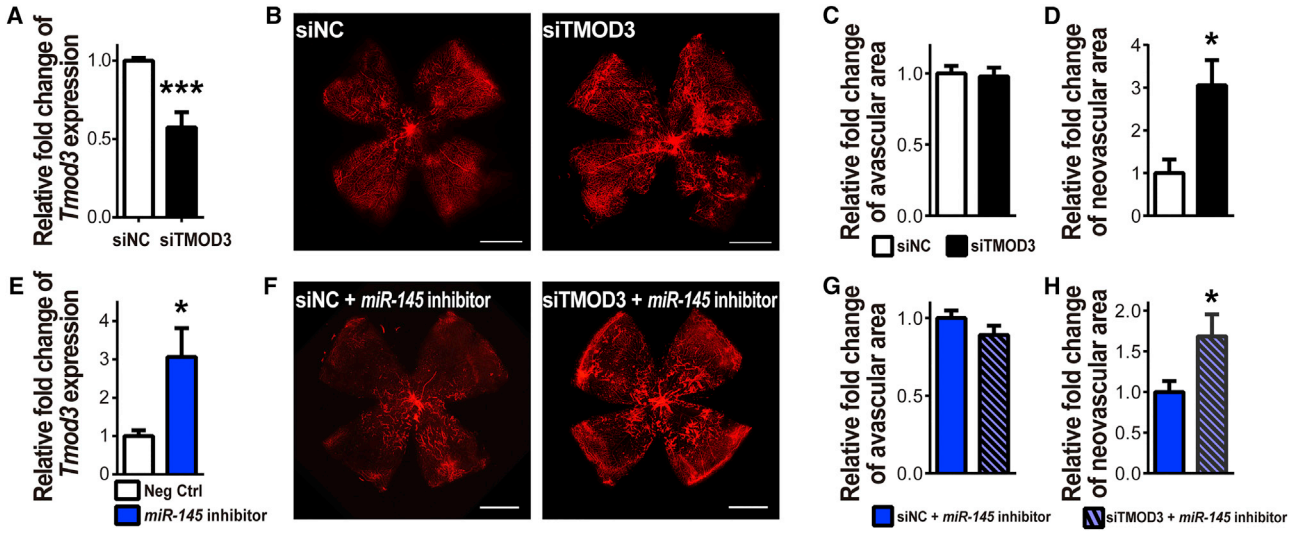

Figure 7. Inhibition of *Tmod3* Increases Pathological Neovascularization in OIR

(A–D) Intravitreal injection of siTMOD3 or siNC was performed in OIR mouse eyes at P12, with siTMOD3 injected in one eye and siNC in the contralateral eye. Efficiency of siTMOD3 was verified by qPCR (A), showing an ~50% reduction of *Tmod3* expression after treating with siTMOD3 in the OIR retinas. Expression levels were normalized to *Gapdh* and to negative controls (n = 4 mice per group). Representative retinal whole mounts stained with IB_4 from P17 OIR mice (B) were used for analysis of retinal pathologic vasculature. Quantification of vaso-obliteration (C) and pathological neovascularization (D) at P17 in OIR showed significantly increased neovascular area with siTMOD3 treatment compared with that in contralateral eyes treated with siNC (D), without a significant difference in vaso-obliteration (C) (n = 7 per group). (E) Retinal *Tmod3* expression was analyzed in P17 OIR retinas with intravitreal injection of *miR-145* inhibitors into one eye and non-targeting negative controls (Neg Ctrl) into the contralateral eye at P12. *Tmod3* expression was significantly increased in OIR retinas treated with *miR-145* inhibitors by ~3-fold. Expression levels were normalized to *Gapdh* and to negative controls (n = 6 mice per group). (F–H) OIR mouse eyes were intravitreally injected with *miR-145* inhibitors combined with siTMOD3 in one eye and siNC in the contralateral eye at P12 after removal from an oxygen chamber. Staining with IB_4 in P17 mouse retinas (F) were used for quantification of vaso-obliteration (G) and neovascularization (H). *miR-145* inhibitor combined with siTMOD3 treatment showed a significant increase in neovascular area in OIR retinas compared with contralateral eyes treated with the siNC-*miR-145* inhibitor cocktail, but no significant effect on vaso-obliteration (n = 8 per group). Scale bars represent 1 mm (B and F). Data are presented as means ± SEM. *$p < 0.05$; ***$p \leq 0.001$.

Dysregulated miRNAs have been associated with abnormal ocular angiogenesis in clinical retinopathy.[10,23,27] This study presents evidence of a novel role of *miR-145* as a regulator of EC morphology and angiogenesis in experimental retinopathy. These findings provide new insight into targeting *miR-145* and the endothelial *miR-145*/TMOD3 axis as potential miRNA-based therapeutic strategies for retinopathy and are also relevant for other vascular diseases associated with pathological angiogenesis. Recently, intravitreal injection of PF-04523655, a synthetic siRNA targeting a stress-induced gene, *RTP801*, was well tolerated in a phase I/IIa study in patients with choroidal neovascularization and neovascular age-related macular degeneration,[53,54] as well as in diabetic macular edema.[55] With respect to post-transcriptional gene repression, the biogenesis and mechanisms of miRNAs are similar to siRNAs,[56] suggesting the future possibility of targeting dysregulated miRNAs via intravitreal injection of miRNA modulators as potential therapeutic options.

MATERIALS AND METHODS

Animals

All animal studies were approved by the Institutional Animal Care and Use Committee at Boston Children's Hospital and adhered to the Association for Research in Vision and Ophthalmology Statement for the Use of Animals in Ophthalmic and Vision Research. C57BL/6J mice (stock no. 000664) were obtained from Jackson Laboratory (Bar Harbor, ME, USA) and used for this study.

OIR Model

The OIR was induced in mice as described previously.[57–59] Briefly, neonatal mice with their nursing mother were exposed to 75% oxygen at P7 for 5 days and then returned to room air at P12. At the selected time points, the mice were sacrificed, followed by enucleation of the eyes for the following experiments.

Intravitreal Injection

For evaluating the effects of *miR-145* and *Tmod3* in pathological angiogenesis, intravitreal injections were performed in OIR mice at P12 after their removal from an oxygen chamber.[23,60] The mice were anesthetized with isoflurane in oxygen from a precision vaporizer for approximately 5 min until they became immobilized. The eyelids were separated, and the eyes were proptosed with gentle pressure. For each mouse, 1 μg of *miR-145* inhibitors (mirVana; Ambion, Thermo Fisher Scientific, Waltham, MA, USA) and/or siRNA targeting *TMOD3* (siTMOD3) (Integrated DNA Technologies, Skokie, IL, USA) dissolved in 0.5 μL of vehicle solution was injected behind the limbus of the eye, and the contralateral eye was injected with an equal amount of negative control RNAs or siRNAs with scrambled

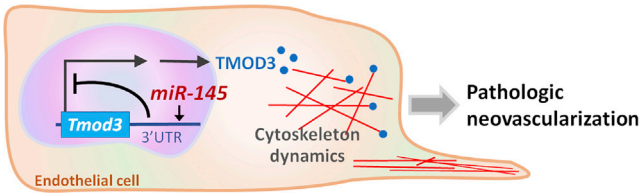

Figure 8. Proposed Role of the *miR-145*-TMOD3 Axis in Proliferative Retinopathy

In normal retinal vessels, endothelial TMOD3 binds to the pointed ends of actin filaments, keeping the cytoskeletal structure steady and maintaining blood vessels in quiescence. In proliferative retinopathy, increased expression of endothelial *miR-145* represses expression of *Tmod3*, resulting in changed dynamics and architecture of actin filaments, which may lead to increased EC sprouting and proliferation, which affect pathological angiogenesis. Inhibition of *miR-145* suppresses neovessel formation in experimental retinopathy.

sequence (siNC), with or without 1 μg of *miR-145* inhibitors. The eyes were lubricated with sterile saline after injection, and an antibiotic eye ointment was applied. After 5 days in room air, the mice were sacrificed at P17, for the study of retinal vasculature.

To verify the effects of *miR-145* during physiological vascular development, anesthesia was induced in neonatal mice at P1, P5, and P6 by placing them indirectly on crushed ice for approximately 5 min until they became immobilized, and the eyes were gently proptosed with fine tweezers. One eye was intravitreally injected with 1 μg *miR-145* inhibitors or mimics (mirVana; Ambion) dissolved in 0.5 μL of vehicle solution in one eye, and the contralateral eye was injected with an equal amount of negative control oligomers. As described previously, topical lubricating solution and occasional antibiotic ointment were applied to the eyes. At P5, P7, or P10, the mice were sacrificed for the study of superficial and deep layers of retinal vasculature.

Retinal Whole Mounts and Quantification of Vasculature

Both vaso-obliteration and pathological neovascularization in the OIR mouse retinas were quantified at P17, as previously described.[57] Briefly, the eyes were fixed with 4% paraformaldehyde dissolved in PBS at room temperature for 1 hour, and the retinas were dissected for overnight incubation with fluorescent *Griffonia simplicifolia* isolectin B_4 (Invitrogen, Thermo Fisher Scientific) and flat mounted. Images of retinal whole mounts were examined by fluorescence microscope (Zeiss AxioOberver.Z1; Carl Zeiss, Oberkochen, Germany). Vascular loss and neovascular areas in OIR were quantified by using Adobe Photoshop (Adobe Systems, San Jose, CA, USA) and ImageJ (NIH, Bethesda, MD, USA; https://imagej.nih.gov/ij/). Vascular density in the developing retinas was analyzed, using the Vessel Analysis plugin with Fiji.[61] Researchers performing quantification of retinal vessels were masked to the identity of samples; n represents the number of eyes quantified.[62]

Aortic Ring Assay

Aortic ring assays were performed as described previously.[63,64] Twenty-day-old mice were euthanized and the aortae were dissected and cut into 1-mm-thick rings, followed by overnight incubation in serum-free medium, then embedded in 30 μL of growth factor-reduced Matrigel (BD Biosciences, Franklin Lakes, NJ, USA) in 24-well tissue culture plates containing Complete Classic Medium (Cell Systems, Kirkland, WA, USA) and incubated at 37°C with 5% CO_2. Medium was changed every other day in all groups. Images of individual explants were taken with a Zeiss AxioOberver.Z1 microscope beginning at 4 days after plating. The vascular sprouting area was quantified with a semi-automated macro plug-in for ImageJ.

Bioinformatics

The conserved seed sequences of *miR-145* from different species, including human and murine, were obtained from miRBase (http://www.mirbase.org/).[65,66] Potential targets of *miR-145* were predicted according to the algorithms of TargetScan v.7 (http://www.targetscan.org/)[67] and microRNA.org (miRanada-mirSVR) (http://www.microrna.org/microrna/home.do/),[68] with incorporation of the context score ++ <−0.2 and mirSVR score <−0.5, respectively.

Real-Time qRT-PCR

Total RNA was extracted from the homogenized retinas of mice or the cultured cells by PureLink RNA Mini Kit (Invitrogen), according to the manufacturer's instructions, followed by synthesis of cDNA by reverse transcription with iScript Reverse Transcriptase (Bio-Rad, Hercules, CA, USA). MicroRNA was isolated from retinas of mice in OIR and normoxia with the miRNeasy Micro Kit (QIAGEN, Hilden, Germany), and the cDNA was generated using the TaqMan miR reverse transcription kit (Applied Biosystems, Thermo Fisher Scientific).

Quantitative analysis of gene expression was determined by qRT-PCR with a C1000 Thermal Cycler (Bio-Rad) and 2× SYBR Green qPCR Master Mix (Bimake.com, Houston, TX, USA) with specific primers. Each target gene cDNA copy number was normalized to the housekeeping gene *S18*, using the comparative CT (ΔΔCT) method. *miR-145* expression level was also analyzed by qPCR with TaqMan miRNA Gene Expression Assays and TaqMan Universal PCR Master Mix (Applied Biosystems), according to the manufacturer's instructions. Data were quantified by ΔΔCT method and normalized to *U6* small nuclear RNA (snRNA) as the endogenous reference. A list of specific primers is summarized in Table S1.

Cell Culture

HRMECs (Cell Systems) were cultured at 37°C and 5% CO_2 in a humid atmosphere in Complete Classic Medium (Cell Systems). HEK293T cells (ATCC, Manassas, VA, USA) were maintain in high-glucose DMEM (Invitrogen) supplemented with 10% fetal bovine serum in 5% CO_2 at 37°C.

Transfection

miR-145 mimics, inhibitors, and non-targeting scrambled negative control RNAs (Ambion), as well as siTMOD3 and siNC (Integrated DNA Technologies, San Jose, CA, USA) were used. Cells or aortic explants were transfected with (1) 25 or 50 nM of *miR-145* mimics,

inhibitors, or negative control RNAs or (2) 50 nM of *miR-145* inhibitors or negative control RNAs combined with 5 or 10 nM of siTMOD3 or siNC, using Lipofectamine 3000 (Invitrogen), according to the manufacturer's instructions. Briefly, synthetic miRNA oligomers or siRNAs were complexed with the transfection reagent in serum-free culture medium and added to cells or aortic explants in fresh full-growth medium. Cells were then used for the following assays after a 24 h transfection.

Tube Formation Assay

HRMECs transfected with various modulators or controls were seeded in a 24-well plate coated with Matrigel (BD Bioscience), at a density of 1×10^5 cells/well. Cells were incubated at 37°C for 6 h and then imaged with a Zeiss AxioObserver.Z1 microscope to assess the formation of tube-like structures. The total mesh area was analyzed by the Angiogenesis Analyzer plug-in for ImageJ[69] (n = 6 per group).

In Vitro Scratch Assay

HRMECs transfected with various modulators or controls were seeded at a concentration of 2×10^5 cells/well. After 24 h of transfection, the cells were treated with 10 μg/mL mitomycin C (Sigma-Aldrich, St. Louis, MO, USA) for 20 min at 37°C. Cell monolayers were wounded by scraping with a pipette tip and incubated at 37°C for 14–18 h. Images of the cells were taken immediately after scraping and again after cell migration into wounded areas. The area covered by the migrating cells was quantified and normalized to the original wound area (n = 6 per group).[70]

MTT Assay

HRMECs transfected with various modulators or controls were seeded at a concentration of 2×10^5 cells/mL into 96-well plates and incubated with DMEM at 37°C for 24 h. Cell proliferative activity was assayed using the Vybrant MTT Cell Proliferation kit (Invitrogen) according to the manufacturer's protocol. Absorbance was read at 570 nm by using the xMark Microplate Spectrophotometer (Bio-Rad).

Luciferase Reporter Assay

The oligonucleotides comprising the *miR-145* target sequences were synthesized by Integrated DNA Technologies and annealed and cloned into the pmirGLO vector (Promega, Madison, WI, USA) for luciferase reporter assays. The *miR-145* target sequences within the 3′ UTR of each target gene were predicted by TargetScan v.7 and microRNA.org, as described previously.[67,68] Constructs containing sequences with the *miR-145* seed-matched sites (Table S2) were confirmed by sequencing at Eton Bioscience (San Diego, CA, USA). HEK293T cells were plated into 96-well plates at 2×10^4 cells/well and transfected with the reporter plasmids containing target sequences or empty vectors as the control, using Lipofectamine 2000 (Invitrogen). Cells were co-transfected with 25 or 50 nM *miR-145* mimics or negative controls (Ambion). After 24 h, luciferase activity was measured, using the Dual-Glo Luciferase Assay System (Promega). Firefly luciferase activity was normalized to *Renilla* luciferase activity and to negative controls.

Hypoxia Treatment in HRMEC Culture

HRMECs were maintained as described in previous sections and allowed to grow until >90% confluence, as inspected visually. To achieve hypoxia, an air mixture (5% CO_2/95% N_2) was used to flush the hypoxia cell culture chamber containing cell culture plates to create a hypoxic condition with <2% O_2, as measured by oxygen sensor. HRMECs were exposed for 6, 12, and 24 h to the hypoxic condition and harvested. Control HRMECs were maintained in normoxia and harvested at 24 h.

Immunofluorescence and Imaging

HRMECs growing on coverslips were fixed with 4% paraformaldehyde at room temperature for 10 min followed by washes in PBS and then blocked with blocking buffer (1× PBS, 5% normal goat serum, and 0.1% Triton X-100) for 30 min. Cells were incubated overnight at 4°C with anti-TMOD3 antibody (1:200 dilution; Aviva Systems Biology, San Diego, CA, USA). After washes in PBS, the cells were incubated with Alexa Fluor 488 goat anti-rabbit IgG antibody (1:200 dilution; Invitrogen), in parallel with rhodamine phalloidin (1:200 dilution; Invitrogen) for 1 hour at room temperature, followed by counterstaining with 4′,6-diamidino-2-phenylindole dihydrochloride (DAPI; Invitrogen). Cells were then rinsed, mounted in mounting medium, and imaged with an inverted Zeiss LSM880 confocal microscope. Cell shape was determined by measuring individual cell length and width, using Adobe Photoshop and ImageJ. The aspect ratio of cell shape denoted the ratio of the maximum length to the maximum width.

Western Blot Analysis

Retinas or cells were lysed in radioimmunoprecipitation assay (RIPA) buffer (Thermo Scientific) with protease and phosphatase inhibitors (Sigma-Aldrich). Lysates then were placed in SDS sample buffer and heated at 100°C for 5 min. Proteins were separated by SDS-PAGE, transferred to polyvinylidene fluoride membranes, and probed with an anti-TMOD3 antibody (Aviva Systems Biology) and anti-glyceraldehyde 3-phosphate dehydrogenase (GAPDH) antibody (Santa Cruz Biotechnology, Dallas, TX, USA). Horseradish peroxidase (HRP)-conjugated anti-mouse IgG and anti-rabbit IgG secondary antibodies (GE Healthcare Life Sciences, Marlborough, MA, USA) were used. Signals were detected with the Novex ECL Chemiluminescent Substrate Reagent Kit (Invitrogen).

Statistical Analysis

Quantitative data are presented as means ± SEM, and asterisks in figures represent the p-value according to the two-tailed Student's t test (two groups) or ANOVA (more than two groups): * $p \leq 0.05$; ** $p \leq 0.005$; *** $p \leq 0.001$.

SUPPLEMENTAL INFORMATION

Supplemental Information can be found online at https://doi.org/10.1016/j.omtn.2019.03.001.

AUTHOR CONTRIBUTIONS

C.-H.L. and J.C. conceived of and designed the study and wrote the manuscript. C.-H.L., Z.W., and S.H. collected and analyzed the

data. Y.S. provided expert advice. All authors edited and approved the manuscript.

CONFLICTS OF INTEREST

The authors declare no competing interests.

ACKNOWLEDGMENTS

This work was supported by the following funders in United States: Knights Templar Eye Foundation under the Pediatric Ophthalmology Career-Starter Research Grant (to C.-H.L.), NIH R01 grants (EY024963 and EY028100), BrightFocus Foundation, Massachusetts Lions Eye Research Fund, Inc., and a Research to Prevent Blindness Dolly Green Special Scholar Award (to J.C.). Z.W. was supported by a Knights Templar Eye Foundation Pediatric Ophthalmology Career-Starter Research Grant and Y.S. was supported by a Boston Children's Hospital Faculty Career Development Award. We thank Rubi Duran, Alexander Poblete, Steve Cho, and William Britton for their excellent technical assistance.

REFERENCES

1. Potente, M., Gerhardt, H., and Carmeliet, P. (2011). Basic and therapeutic aspects of angiogenesis. Cell *146*, 873–887.
2. Folkman, J. (1995). Angiogenesis in cancer, vascular, rheumatoid and other disease. Nat. Med. *1*, 27–31.
3. Afzal, A., Shaw, L.C., Ljubimov, A.V., Boulton, M.E., Segal, M.S., and Grant, M.B. (2007). Retinal and choroidal microangiopathies: therapeutic opportunities. Microvasc. Res. *74*, 131–144.
4. Gerhardt, H., Golding, M., Fruttiger, M., Ruhrberg, C., Lundkvist, A., Abramsson, A., Jeltsch, M., Mitchell, C., Alitalo, K., Shima, D., and Betsholtz, C. (2003). VEGF guides angiogenic sprouting utilizing endothelial tip cell filopodia. J. Cell Biol. *161*, 1163–1177.
5. Crawford, Y., and Ferrara, N. (2009). VEGF inhibition: insights from preclinical and clinical studies. Cell Tissue Res. *335*, 261–269.
6. Darlow, B.A., Ells, A.L., Gilbert, C.E., Gole, G.A., and Quinn, G.E. (2013). Are we there yet? Bevacizumab therapy for retinopathy of prematurity. Arch. Dis. Child. Fetal Neonatal Ed. *98*, F170–F174.
7. Hu, J., Blair, M.P., Shapiro, M.J., Lichtenstein, S.J., Galasso, J.M., and Kapur, R. (2012). Reactivation of retinopathy of prematurity after bevacizumab injection. Arch. Ophthalmol. *130*, 1000–1006.
8. Wallace, D.K., and Wu, K.Y. (2013). Current and future trends in treatment of severe retinopathy of prematurity. Clin. Perinatol. *40*, 297–310.
9. He, L., and Hannon, G.J. (2004). MicroRNAs: small RNAs with a big role in gene regulation. Nat. Rev. Genet. *5*, 522–531.
10. Agrawal, S., and Chaqour, B. (2014). MicroRNA signature and function in retinal neovascularization. World J. Biol. Chem. *5*, 1–11.
11. Brennecke, J., Hipfner, D.R., Stark, A., Russell, R.B., and Cohen, S.M. (2003). bantam encodes a developmentally regulated microRNA that controls cell proliferation and regulates the proapoptotic gene hid in Drosophila. Cell *113*, 25–36.
12. Chang, T.C., and Mendell, J.T. (2007). microRNAs in vertebrate physiology and human disease. Annu. Rev. Genomics Hum. Genet. *8*, 215–239.
13. Im, H.I., and Kenny, P.J. (2012). MicroRNAs in neuronal function and dysfunction. Trends Neurosci. *35*, 325–334.
14. Krek, A., Grün, D., Poy, M.N., Wolf, R., Rosenberg, L., Epstein, E.J., MacMenamin, P., da Piedade, I., Gunsalus, K.C., Stoffel, M., and Rajewsky, N. (2005). Combinatorial microRNA target predictions. Nat. Genet. *37*, 495–500.
15. Lim, L.P., Lau, N.C., Garrett-Engele, P., Grimson, A., Schelter, J.M., Castle, J., Bartel, D.P., Linsley, P.S., and Johnson, J.M. (2005). Microarray analysis shows that some microRNAs downregulate large numbers of target mRNAs. Nature *433*, 769–773.
16. Anand, S., and Cheresh, D.A. (2011). Emerging Role of Micro-RNAs in the Regulation of Angiogenesis. Genes Cancer *2*, 1134–1138.
17. Anand, S., Majeti, B.K., Acevedo, L.M., Murphy, E.A., Mukthavaram, R., Scheppke, L., Huang, M., Shields, D.J., Lindquist, J.N., Lapinski, P.E., et al. (2010). MicroRNA-132-mediated loss of p120RasGAP activates the endothelium to facilitate pathological angiogenesis. Nat. Med. *16*, 909–914.
18. Nicoli, S., Standley, C., Walker, P., Hurlstone, A., Fogarty, K.E., and Lawson, N.D. (2010). MicroRNA-mediated integration of haemodynamics and Vegf signalling during angiogenesis. Nature *464*, 1196–1200.
19. Png, K.J., Halberg, N., Yoshida, M., and Tavazoie, S.F. (2011). A microRNA regulon that mediates endothelial recruitment and metastasis by cancer cells. Nature *481*, 190–194.
20. Shen, J., Yang, X., Xie, B., Chen, Y., Swaim, M., Hackett, S.F., and Campochiaro, P.A. (2008). MicroRNAs regulate ocular neovascularization. Mol. Ther. *16*, 1208–1216.
21. Poliseno, L., Tuccoli, A., Mariani, L., Evangelista, M., Citti, L., Woods, K., Mercatanti, A., Hammond, S., and Rainaldi, G. (2006). MicroRNAs modulate the angiogenic properties of HUVECs. Blood *108*, 3068–3071.
22. Wang, S., and Olson, E.N. (2009). AngiomiRs: key regulators of angiogenesis. Curr. Opin. Genet. Dev. *19*, 205–211.
23. Liu, C.H., Sun, Y., Li, J., Gong, Y., Tian, K.T., Evans, L.P., Morss, P.C., Fredrick, T.W., Saba, N.J., and Chen, J. (2015). Endothelial microRNA-150 is an intrinsic suppressor of pathologic ocular neovascularization. Proc. Natl. Acad. Sci. USA *112*, 12163–12168.
24. Westenskow, P.D., Kurihara, T., Aguilar, E., Scheppke, E.L., Moreno, S.K., Wittgrove, C., Marchetti, V., Michael, I.P., Anand, S., Nagy, A., et al. (2013). Ras pathway inhibition prevents neovascularization by repressing endothelial cell sprouting. J. Clin. Invest. *123*, 4900–4908.
25. Wang, S., Aurora, A.B., Johnson, B.A., Qi, X., McAnally, J., Hill, J.A., Richardson, J.A., Bassel-Duby, R., and Olson, E.N. (2008). The endothelial-specific microRNA miR-126 governs vascular integrity and angiogenesis. Dev. Cell *15*, 261–271.
26. Zhou, Q., Gallagher, R., Ufret-Vincenty, R., Li, X., Olson, E.N., and Wang, S. (2011). Regulation of angiogenesis and choroidal neovascularization by members of microRNA-23∼27∼24 clusters. Proc. Natl. Acad. Sci. USA *108*, 8287–8292.
27. Liu, C.H., Wang, Z., Sun, Y., SanGiovanni, J.P., and Chen, J. (2016). Retinal expression of small non-coding RNAs in a murine model of proliferative retinopathy. Sci. Rep. *6*, 33947.
28. Kent, O.A., McCall, M.N., Cornish, T.C., and Halushka, M.K. (2014). Lessons from miR-143/145: the importance of cell-type localization of miRNAs. Nucleic Acids Res. *42*, 7528–7538.
29. Xin, M., Small, E.M., Sutherland, L.B., Qi, X., McAnally, J., Plato, C.F., Richardson, J.A., Bassel-Duby, R., and Olson, E.N. (2009). MicroRNAs miR-143 and miR-145 modulate cytoskeletal dynamics and responsiveness of smooth muscle cells to injury. Genes Dev. *23*, 2166–2178.
30. Dimitrova, N., Gocheva, V., Bhutkar, A., Resnick, R., Jong, R.M., Miller, K.M., Bendor, J., and Jacks, T. (2016). Stromal Expression of miR-143/145 Promotes Neoangiogenesis in Lung Cancer Development. Cancer Discov. *6*, 188–201.
31. Lee, S.K., Teng, Y., Wong, H.K., Ng, T.K., Huang, L., Lei, P., Choy, K.W., Liu, Y., Zhang, M., Lam, D.S., et al. (2011). MicroRNA-145 regulates human corneal epithelial differentiation. PLoS ONE *6*, e21249.
32. Li, X., Zhao, F., Xin, M., Li, G., Luna, C., Li, G., Zhou, Q., He, Y., Yu, B., Olson, E., et al. (2017). Regulation of intraocular pressure by microRNA cluster miR-143/145. Sci. Rep. *7*, 915.
33. Stahl, A., Connor, K.M., Sapieha, P., Chen, J., Dennison, R.J., Krah, N.M., Seaward, M.R., Willett, K.L., Aderman, C.M., Guerin, K.I., et al. (2010). The mouse retina as an angiogenesis model. Invest. Ophthalmol. Vis. Sci. *51*, 2813–2826.
34. Lewis, B.P., Burge, C.B., and Bartel, D.P. (2005). Conserved seed pairing, often flanked by adenosines, indicates that thousands of human genes are microRNA targets. Cell *120*, 15–20.
35. Yamashiro, S., Gokhin, D.S., Kimura, S., Nowak, R.B., and Fowler, V.M. (2012). Tropomodulins: pointed-end capping proteins that regulate actin filament architecture in diverse cell types. Cytoskeleton (Hoboken) *69*, 337–370.

36. Fischer, R.S., Fritz-Six, K.L., and Fowler, V.M. (2003). Pointed-end capping by tropomodulin3 negatively regulates endothelial cell motility. J. Cell Biol. *161*, 371–380.

37. Dodeller, F., Gottar, M., Huesken, D., Iourgenko, V., and Cenni, B. (2008). The lysosomal transmembrane protein 9B regulates the activity of inflammatory signaling pathways. J. Biol. Chem. *283*, 21487–21494.

38. Blick, C., Ramachandran, A., McCormick, R., Wigfield, S., Cranston, D., Catto, J., and Harris, A.L. (2015). Identification of a hypoxia-regulated miRNA signature in bladder cancer and a role for miR-145 in hypoxia-dependent apoptosis. Br. J. Cancer *113*, 634–644.

39. Hartnett, M.E., and Penn, J.S. (2012). Mechanisms and management of retinopathy of prematurity. N. Engl. J. Med. *367*, 2515–2526.

40. Boucher, J.M., Peterson, S.M., Urs, S., Zhang, C., and Liaw, L. (2011). The miR-143/145 cluster is a novel transcriptional target of Jagged-1/Notch signaling in vascular smooth muscle cells. J. Biol. Chem. *286*, 28312–28321.

41. Lobov, I.B., Cheung, E., Wudali, R., Cao, J., Halasz, G., Wei, Y., Economides, A., Lin, H.C., Papadopoulos, N., Yancopoulos, G.D., and Wiegand, S.J. (2011). The Dll4/Notch pathway controls postangiogenic blood vessel remodeling and regression by modulating vasoconstriction and blood flow. Blood *117*, 6728–6737.

42. Weinl, C., Riehle, H., Park, D., Stritt, C., Beck, S., Huber, G., Wolburg, H., Olson, E.N., Seeliger, M.W., Adams, R.H., and Nordheim, A. (2013). Endothelial SRF/MRTF ablation causes vascular disease phenotypes in murine retinae. J. Clin. Invest. *123*, 2193–2206.

43. Hellström, M., Phng, L.K., Hofmann, J.J., Wallgard, E., Coultas, L., Lindblom, P., Alva, J., Nilsson, A.K., Karlsson, L., Gaiano, N., et al. (2007). Dll4 signalling through Notch1 regulates formation of tip cells during angiogenesis. Nature *445*, 776–780.

44. Franco, C.A., Blanc, J., Parlakian, A., Blanco, R., Aspalter, I.M., Kazakova, N., Diguet, N., Mylonas, E., Gao-Li, J., Vaahtokari, A., et al. (2013). SRF selectively controls tip cell invasive behavior in angiogenesis. Development *140*, 2321–2333.

45. Bao, Z.Z., and Cepko, C.L. (1997). The expression and function of Notch pathway genes in the developing rat eye. J. Neurosci. *17*, 1425–1434.

46. Benedito, R., Roca, C., Sörensen, I., Adams, S., Gossler, A., Fruttiger, M., and Adams, R.H. (2009). The notch ligands Dll4 and Jagged1 have opposing effects on angiogenesis. Cell *137*, 1124–1135.

47. Cheng, Y., Liu, X., Yang, J., Lin, Y., Xu, D.Z., Lu, Q., Deitch, E.A., Huo, Y., Delphin, E.S., and Zhang, C. (2009). MicroRNA-145, a novel smooth muscle cell phenotypic marker and modulator, controls vascular neointimal lesion formation. Circ. Res. *105*, 158–166.

48. Ji, R., Cheng, Y., Yue, J., Yang, J., Liu, X., Chen, H., Dean, D.B., and Zhang, C. (2007). MicroRNA expression signature and antisense-mediated depletion reveal an essential role of MicroRNA in vascular neointimal lesion formation. Circ. Res. *100*, 1579–1588.

49. Pollard, T.D., and Borisy, G.G. (2003). Cellular motility driven by assembly and disassembly of actin filaments. Cell *112*, 453–465.

50. Lim, C.Y., Bi, X., Wu, D., Kim, J.B., Gunning, P.W., Hong, W., and Han, W. (2015). Tropomodulin3 is a novel Akt2 effector regulating insulin-stimulated GLUT4 exocytosis through cortical actin remodeling. Nat. Commun. *6*, 5951.

51. Quintero, H., Gómez-Montalvo, A.I., and Lamas, M. (2016). MicroRNA changes through Müller glia dedifferentiation and early/late rod photoreceptor differentiation. Neuroscience *316*, 109–121.

52. Ratuszny, D., Gras, C., Bajor, A., Börger, A.K., Pielen, A., Börgel, M., Framme, C., Blasczyk, R., and Figueiredo, C. (2015). miR-145 Is a Promising Therapeutic Target to Prevent Cornea Scarring. Hum. Gene Ther. *26*, 698–707.

53. Hanout, M., Ferraz, D., Ansari, M., Maqsood, N., Kherani, S., Sepah, Y.J., Rajagopalan, N., Ibrahim, M., Do, D.V., and Nguyen, Q.D. (2013). Therapies for neovascular age-related macular degeneration: current approaches and pharmacologic agents in development. BioMed Res. Int. *2013*, 830837.

54. PF-04523655 Study Group (2012). Phase 1 dose-escalation study of a siRNA targeting the RTP801 gene in age-related macular degeneration patients. Eye (Lond.) *26*, 1099–1105.

55. DEGAS Clinical Study Group (2012). Dose-ranging evaluation of intravitreal siRNA PF-04523655 for diabetic macular edema (the DEGAS study). Invest. Ophthalmol. Vis. Sci. *53*, 7666–7674.

56. Chakraborty, C., Sharma, A.R., Sharma, G., Doss, C.G.P., and Lee, S.S. (2017). Therapeutic miRNA and siRNA: Moving from Bench to Clinic as Next Generation Medicine. Mol. Ther. Nucleic Acids *8*, 132–143.

57. Connor, K.M., Krah, N.M., Dennison, R.J., Aderman, C.M., Chen, J., Guerin, K.I., Sapieha, P., Stahl, A., Willett, K.L., and Smith, L.E. (2009). Quantification of oxygen-induced retinopathy in the mouse: a model of vessel loss, vessel regrowth and pathological angiogenesis. Nat. Protoc. *4*, 1565–1573.

58. Smith, L.E., Wesolowski, E., McLellan, A., Kostyk, S.K., D'Amato, R., Sullivan, R., and D'Amore, P.A. (1994). Oxygen-induced retinopathy in the mouse. Invest. Ophthalmol. Vis. Sci. *35*, 101–111.

59. Liu, C.H., Wang, Z., Sun, Y., and Chen, J. (2017). Animal models of ocular angiogenesis: from development to pathologies. FASEB J. *31*, 4665–4681.

60. Chen, J., Connor, K.M., Aderman, C.M., Willett, K.L., Aspegren, O.P., and Smith, L.E. (2009). Suppression of retinal neovascularization by erythropoietin siRNA in a mouse model of proliferative retinopathy. Invest. Ophthalmol. Vis. Sci. *50*, 1329–1335.

61. Schindelin, J., Arganda-Carreras, I., Frise, E., Kaynig, V., Longair, M., Pietzsch, T., Preibisch, S., Rueden, C., Saalfeld, S., Schmid, B., et al. (2012). Fiji: an open-source platform for biological-image analysis. Nat. Methods *9*, 676–682.

62. Stahl, A., Connor, K.M., Sapieha, P., Willett, K.L., Krah, N.M., Dennison, R.J., Chen, J., Guerin, K.I., and Smith, L.E. (2009). Computer-aided quantification of retinal neovascularization. Angiogenesis *12*, 297–301.

63. Baker, M., Robinson, S.D., Lechertier, T., Barber, P.R., Tavora, B., D'Amico, G., Jones, D.T., Vojnovic, B., and Hodivala-Dilke, K. (2011). Use of the mouse aortic ring assay to study angiogenesis. Nat. Protoc. *7*, 89–104.

64. Li, J., Liu, C.H., Sun, Y., Gong, Y., Fu, Z., Evans, L.P., Tian, K.T., Juan, A.M., Hurst, C.G., Mammoto, A., and Chen, J. (2014). Endothelial TWIST1 promotes pathological ocular angiogenesis. Invest. Ophthalmol. Vis. Sci. *55*, 8267–8277.

65. Griffiths-Jones, S., Grocock, R.J., van Dongen, S., Bateman, A., and Enright, A.J. (2006). miRBase: microRNA sequences, targets and gene nomenclature. Nucleic Acids Res. *34*, D140–D144.

66. Kozomara, A., and Griffiths-Jones, S. (2014). miRBase: annotating high confidence microRNAs using deep sequencing data. Nucleic Acids Res. *42*, D68–D73.

67. Agarwal, V., Bell, G.W., Nam, J.W., and Bartel, D.P. (2015). Predicting effective microRNA target sites in mammalian mRNAs. eLife *4*, 05005.

68. Betel, D., Koppal, A., Agius, P., Sander, C., and Leslie, C. (2010). Comprehensive modeling of microRNA targets predicts functional non-conserved and non-canonical sites. Genome Biol. *11*, R90.

69. Carpentier, G., Martinelli, M., Courty, J., and Cascone, I. (2012). Angiogenesis Analyzer for ImageJ. Proceedings of the 4th ImageJ User and Developer Conference (Luxembourg Institute of Science and Technology), pp. 198–201.

70. Gong, Y., Yang, X., He, Q., Gower, L., Prudovsky, I., Vary, C.P., Brooks, P.C., and Friesel, R.E. (2013). Sprouty4 regulates endothelial cell migration via modulating integrin β3 stability through c-Src. Angiogenesis *16*, 861–875.

OMTN, Volume *16*

Supplemental Information

MicroRNA-145 Regulates Pathological Retinal Angiogenesis by Suppression of TMOD3

Chi-Hsiu Liu, Zhongxiao Wang, Shuo Huang, Ye Sun, and Jing Chen

Supplemental Information

MicroRNA-145 regulates pathological retinal angiogenesis by suppression of TMOD3

Chi-Hsiu Liu, Zhongxiao Wang, Shuo Huang, Ye Sun and Jing Chen*

Department of Ophthalmology, Boston Children's Hospital, Harvard Medical School, Boston, Massachusetts 02115, USA

*Corresponding author should be addressed to J. C. (jing.chen@childrens.harvard.edu)

Table S1. Primers for q-PCR

Gene	Forward (5'→3')	Reverse (5'→3')
Mouse		
c-Myc	GGATTGGGCTACGGAGATGCT	ATGACCGGATTAGGAGTGAAG
Gapdh	GCCTACATG GCCTCCAAGG	GAGTTGGGATAGGGCCTCTCTT
Klf4	GTGCCCCGACTAACCGTTG	GTCGTTGAACTCCTCGGTCT
Sema3a	TGACGCCCAGCCAGAAGGTCT	AGAGTGCCCCGGCCTTTGTC
Tmem9b	CTATGGTGCGGAAACCTGCT	GCCCAGGATTCTCTTTATAGGGA
Tmod3	CTCCTTGGCAAGCTGTCCG	CCCGTGGCAGACTTTGATGT
Trio	AGTCTGAGCACATTGTGTCCG	GCACGATGCACATGACTTCTA
18S	TGCTGCAGTTAAAAAGCTCGT	GGCCTGCTTTGAACACTCTAA
Human		
TMOD3	GTGACCTCGCAGCAATTCTTG	GTGGCTCATCAAATACCGGAA
18S	ACGGAAGGGCACCACCAGGA	CACCACCACCCACGGAATCG

Table S2. Oligonucleotide sequences for luciferase reporter constructs

Gene	NCBI Ref_Seq Accession Number	Seed Position	Sequences (5'→3')*
Klf4	NM_010637.3	+2,399…+2,405	AAATGCCAAGGGGTG**ACTGGAA**GTTTGTGGATATCAGGGT
Sema3a	NM_001243072.1	+2,751…+2,757	ACTTGCTTAGATAAT**AACTGGA**AAAAATGCAATACAC
		+5,573…+5,579	AGATGGGAACTAGAA**AACTGGA**GAGAAAAATGTAACG
Tmem9b	NM_020050.1	+691…+697	CCTCAGCTAACTGGG**AACTGGA**ATCAGGTGACTAGGAAG
		+810…+816	TGGAGGAAGACTCCA**AACTGGA**AGCAAACCCCATGCTTGGTAT
Tmod3	NM_016963.2	+1,345…+1,351	GGGTAGAAGGGAAAG**ACTGGAA**ATCTTTTTTAACTATATG
Trio	NM_001081302.1	+10,797…+10,803	ATACTCTGAATATAA**AACTGGA**TAATAGGGTAATGTTTTAA
		+11,299…+11,305	GAAATTGGATTCAAA**AACTGGA**TGTGTATCTGTAACCTCA

*The *mmu-miR-145* seed sequence-matched sites are underlined.